Use of Optical Probes to Characterize Bubble Behavior in Gas-Solid Fluidized Beds

Marlene E. Mainland and James R. Welty
Dept. of Mechanical Engineering, Oregon State University, Corvallis, OR 97331

Optical probes are used to study gas-solid fluidized-bed hydrodynamics. The probes each consisting of a light source and photodetector separated by a gap are suitable for use at combustion-level temperatures. The methodology to process the signal for calculation of bubble properties such as bubble frequency, local bubble residence time, bubble velocity, pierced length, bubble size, and visible bubble flow is presented. The signal processing technique is independent of bed operating conditions. The probe signal processing methodology is validated by comparing calculated bubble properties based on the probe signal with properties observed on videotapes of a 2-D bed.

Introduction

Gas-solid fluidized beds are useful for operations involving solid-fluid contacting whenever high rates of heat and mass transfer between solid and fluid are required. Applications of fluidized beds include fluidized-bed coal combustion, the removal of small concentrations of solvents from large quantities of air, processes involving the drying of solids, coating of solids, particle growth, and synthesis gas production.

As the fluidizing velocity in the bed is increased in excess of the minimum fluidization velocity, voids or "bubbles" form and pass upward through the bed. The detection and characterization of bubble behavior are important in understanding fluidized-bed performance.

Due to the stochastic nature of a bubbling bed, it is difficult to achieve meaningful information based on first principles, and most of the reliable information about bubbles is empirical in nature. X-ray photography (Hager and Thomson, 1973; Rowe and Partridge, 1965) provides some information on bubbles, but is limited to beds containing a low concentration of bubbles. Cine photography and videotape (Kunii et al., 1967; Weihong et al., 1987) are useful, however, they are limited by the need for visual access to the bed and the requirement for an abundance of pictures to be taken and analyzed.

Several types of intrusive probes have been discussed earlier which measure bubble properties. Their operations are based on a variety of physical effects such as temperature, resistivity, capacitance, inductance, and pressure changes between dense phase and bubble phase. Several probe concepts possess certain operational limitations. Hot-wire probes (Tsutsui and Miyauchi, 1980) might not be sturdy enough for placement in a bed composed of large particles. Electrical resistivity probes (Matsuura and Fan, 1984; Yoshida et al., 1982; Park et al., 1969) can only be used with liquids and conductive solids. Inductance probes (Cranfield, 1972) use a magnetic field, and bed materials must consequently have magnetic properties. Capacitance probes have been used in fluidized-bed applications with some success (Geldart and Kelsey, 1991; Werther and Molerus, 1973; Gunn and Al-Doori, 1985). A serious shortcoming of capacitance probes is that they must be calibrated for every fluid-solid system and operating condition (in particular temperature and pressure). Probes based on sensing local electrical properties of the fluidized bed would be cumbersome to use in beds that operate over a range of temperatures and particle compositions such as the case in fluidized-bed combustion. Pressure differential probes have been shown to be useful for determining bubble properties (Sitnai, 1982; Venkata, 1993), but the interpretation of the pressure records needs more extensive experimental validation. Fiber-optic (Lasa et al., 1984; Lord et al., 1982) and optical probes (Rowe and Masson, 1981; Yasui and Johanson, 1958; Dutta and Wen, 1979; Masson and Jottrand, 1978; Katoh et al., 1991) have also been introduced, but these have shortcomings such as excessive intrusion in the flow pattern, unsuitability for high-temperature use, and incomplete signal interpretation methodology.

In this work, an optical probe and its use in a two-dimensional (2-D) bed are described. The optical probe is suitable for both low- and high-temperature conditions and is not sensitive to the temperature or physical properties of the fluid-

Correspondence concerning this article should be addressed to M. E. Mainland.

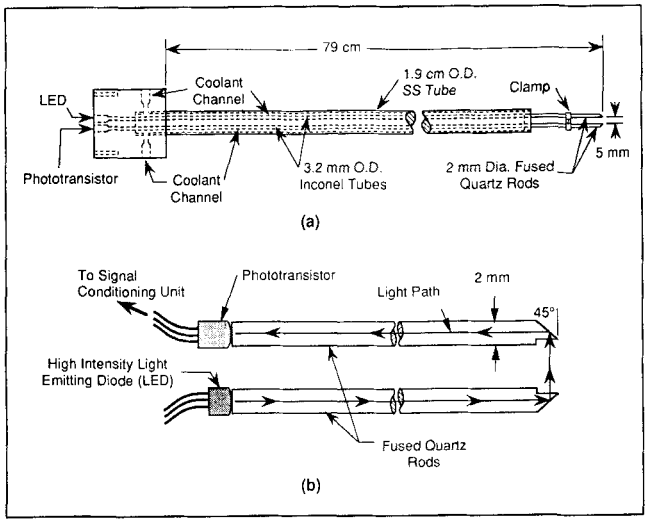

Figure 1. Optical probe (a) and fused quartz rods (b).

solid constituents of the bed. The methodology has been developed for filtering the probe signal and calculating bubble properties such as bubble frequency, local bubble residence time, bubble velocity, pierced length, bubble size, and visible bubble flow. The bubble information obtained from the probe signal was confirmed by comparison with visual information (videotape) of the 2-D bed. A complete knowledge of the information contained in the probe signals provides the basis for these probes to be used in a 3-D high temperature fluidized bed when visual observation is not possible.

Optical Probe

The optical probe unit is shown in Figure 1. Infrared light (880 nm spectral peak) is produced by a high-intensity light emitting diode (LED). The light travels down a fused quartz rod, is reflected across a gap, is reflected down a second rod, and is subsequently incident on a silicon infrared phototransistor matched to the LED. The excitation current to the LED is provided as a square wave at approximately 10 kHz with a constant nominal current large enough that the supplied current is never negative. A periodic signal is used so that radiant emission from a high-temperature bed and other noise can be removed. The phototransistor output is processed using amplitude modulation (Doeblin, 1991). The amplitude-modulated signal contains useful bubble information at the corresponding side frequencies of the 10 kHz carrier signal. This signal is high-pass filtered to remove 50 or 60 Hz noise pickup due to AC power lines, as well as the constant or slowly fluctuating component of the phototransistor output due to radiant emission from a high-temperature bed. The remaining square-wave signal is amplified, full-wave rectified, and filtered to yield a voltage which can be recorded by an oscillograph or a digital data acquisition system. Essentially all of the signal retained after the conditioning has its source at the LED and is not due to radiant emission from a high-temperature bed, as transmitted to the phototransistor through the quartz rods.

For common gas-fluidized systems, the bubble phase is essentially optically clear, and light will be transmitted across the gap to the photodetector when a bubble occupies the gap. Assuming opaque particles (or at least particles which sufficiently scatter light), essentially no transmission of light occurs across the gap when the dense (emulsion) phase fills the gap. The signal was amplified so that the voltage range is approximately 0-3.0 V. The frequency response of the optical probe and signal conditioning unit was experimentally found to be approximately 125 Hz.

The rods, LED, and phototransistor are encased in stainless steel coolant channels suitable for high-temperature operation. The fused quartz rods can operate at combustion level temperatures without softening or undergoing a significant loss of transmittance at infrared wavelengths. To demonstrate their suitability for use at combustion-level temperatures, the probes were tested in a high-temperature furnace with coolant water supplied to the probes. For temperatures ranging from 290 to 1,200 K, the open gap voltage remained essentially constant within approximately $\pm 10\%$ of the room temperature value. Additionally, the sensitivity of the phototransistor was found to be essentially unaffected by the radiant emission from the high-temperature environment. After dozens of hours of operation in a fluidized bed at 660 K when the quartz tips of the probe were subjected to abrasion by the bed particles, the calibration of the probe remained essentially constant.

Experiments

Experiments were run at approximately 313 K and atmospheric pressure in a 2-D fluidized bed. The test section was rectangular in shape with a width of 68.6 cm, a height of 45.7 cm, and a thickness of 3.2 cm. The distributor plate was a 3.2-mm-thick aluminum sheet with 3 rows of 55 holes, 2.38 mm in diameter, and spaced 1.27 cm between centers. The front of the test section was 3.1-mm-thick scratch-resistant plexiglass to allow visual observation. The bed material consisted of silica-alumina particles having a density of 2,700 kg/m^3 and a nominal diameter of 2.0 mm. The packed bed was 30.5 cm deep and the minimum fluidization velocity was found to be $U_{mf} = 115$ cm/s. Two optical probes were mounted horizontally through the back of the test section. The lower probe was located 15.2 cm above the distributor plate, and the second probe was located 5.1 cm above the lower probe. Data were taken over a range of fluidization velocities from minimum fluidization velocity (U_{mf}) to 1.6 U_{mf} with increments of 0.1 U_{mf}. Five data sets were taken at each fluidization velocity for a period of 163 s each. The sampling rate was 200 Hz. The data taking and signal processing were performed on a digital computer.

Probe Signal Processing Methodology

Typical raw probe signals are shown in Figure 2 for $U/U_{mf} = 1.4$. Results obtained for $U/U_{mf} = 1.4$ are representative of the other fluidization velocities employed. While in principle the probe delivers an "on-off" signal, the real analog signal varies from this for two reasons. First, the bubbles contain particles which block the light and reduce the voltage below its maximum "on" value. The particle occurrence inside bubbles is more pronounced in a 2-D bed than a 3-D bed because of the wall effect. Secondly, the voidage in the dense phase adjacent to a bubble can be large (Lockett and Harrison, 1967), which could allow some light to travel across the probe

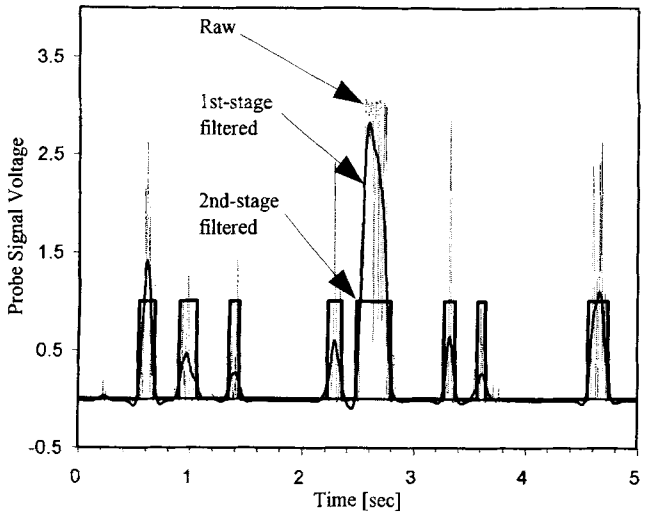

Figure 2. Raw, first-stage-, and second-stage-filtered probe signal for $U/U_{mf}=1.4$.

gap. As bubble properties were of interest in our work, it was necessary to remove particle effects from the signal. This was accomplished by two-stage filtering the raw signal such that the relatively low-frequency bubble information was retained and the higher-frequency particle effect was removed. The two-stage filter consisted of a digital low-pass filter followed by a digital amplitude-cutoff filter.

The first-stage, low-pass filtering was done in the frequency domain following the procedure discussed in Press et al. (1989). The filter selected was a second-order magnitude-squared Butterworth (Johnson, 1976) filter having the following transfer function:

$$H(s)=\left|\frac{1}{s^2+\sqrt{2}s+1}\right|^2 \tag{1}$$

where $s=j\omega/\omega_{cut}$ and $j=\sqrt{-1}$. This filter is used instead of an ideal filter (one having a step change from 1 to 0 at ω_{cut}), because an ideal filter can cause Gibbs phenomena (Walker, 1991) resulting in signal distortion when the inverse transform is performed. The cutoff frequency selected was $\omega_{cut}=7$ Hz. The effect of this filter on the raw signal is shown in Figure 2.

The second-stage filter was an "on-off" amplitude cutoff filter and was used in the time domain. A cutoff voltage v_{cut} was calculated and then values of the first-stage-filtered signal above v_{cut} were assigned a value of 1 ("on") while those below v_{cut} were assigned a value of 0 ("off"). The value of v_{cut} was determined using the following relation:

$$v_{cut}=0.05(v_{max}-v_{min}) \tag{2}$$

where v_{max} and v_{min} were the maximum and minimum values of the first-stage-filtered data, respectively. The resulting signal, shown in Figure 2, has a value of 1 when the probe is immersed in a bubble and a value of 0 when the probe is immersed in the dense phase.

A satisfactory filter is one that eliminates extraneous particle effects yet retains the bubble information. Whenever there is a positive voltage, there is a void (either a bubble or a high-void-fraction region) and whenever the voltage is zero, particles occupy the gap. When two bubbles are very close, it is subjective whether to consider them as one or two bubbles. The assignment of the bubble boundary location is also subjective due to the high void fraction region at the boundary and the large particle content in the bubbles. This is the nature of two-phase flow; the goal is to quantify bubble behavior with the greatest accuracy possible so that their properties can be related to a heat- and/or mass-transfer process of interest. A filter which appeared to capture as much information as possible was therefore selected. So long as the filtered signal appears to capture the desired information (by comparing the raw signal to the filtered signal and considering the comments above), then the resultant bubble properties are not overly sensitive to the value of the filter parameters. Note that the uncertainty associated with observed bubble properties arises primarily from these inherent bubble characteristics.

Calculation of Bubble Properties

Bubble frequency

The bubble frequency was found simply by dividing the number of bubble occurrences by the experiment time duration. Frequency calculations using the probe signal agreed closely with the visually-observed frequency. The probe information was more accurate, because the probe will respond to any void through which light can pass. It was sometimes difficult, however, to determine if the probe was intercepting a bubble by observing the videotape, due to the inherent uncertainty in observations discussed above and since the probe was located 1.6 cm from the plexiglass.

Local bubble residence times

The local bubble residence time is the time the probe is immersed in a bubble during the passage of that bubble (emulsion phase residence time can be calculated similarly). A comparison of values obtained using the probe and those observed is shown in Figure 3 for $U/U_{mf}=1.2$, 1.4, and 1.6. The observed value contains uncertainty due to inexact assignment of the bubble boundary and the time resolution of the videotape, which is between one field and one frame (16.7–33.3 m s). The fraction of total time the probe is immersed in the bubble or emulsion phase can also be calculated.

Bubble velocity

The bubble velocity is a difficult parameter to specify since bubbles collapse, coalesce, have horizontal components of velocity, and have inexact boundaries. Werther (1974) showed that the instantaneous rise velocity of a bubble is a stochastic quantity and that the measurement of individual rise velocities is pointless. Instead of calculating individual rise velocities, a mean bubble velocity was found by cross-correlating the two filtered probe signals. If the upper probe signal is a close copy of the lower probe signal lagging by a time difference t_{cc}, then the cross-correlation function will be a maximum at t_{cc} (Press et al., 1989). The distance between the two probes divided by t_{cc} is the mean bubble velocity. The bubble velocity calculated using the cross-correlation was compared to the relative fre-

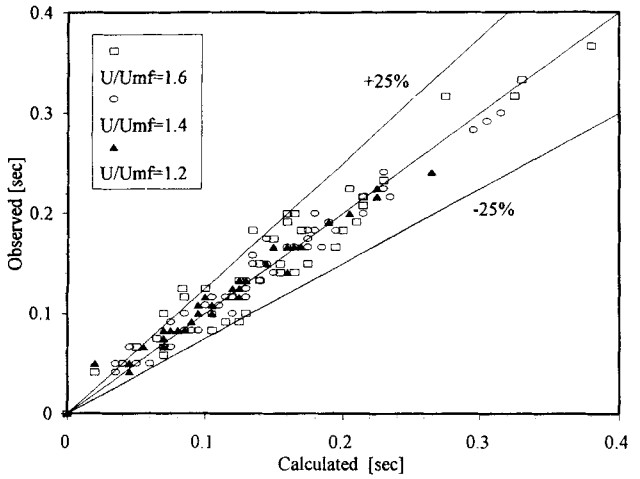

Figure 3. Comparison of calculated and observed local bubble residence times.

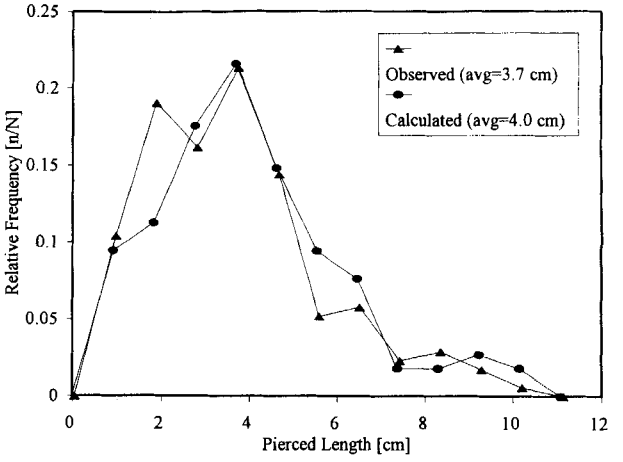

Figure 5. Observed and calculated pierced length relative frequency polygons.

quency polygon of observed bubble velocities in Figure 4 for $U/U_{mf}=1.4$. There was excellent agreement relative to the uncertainty in the observed values as discussed above.

Pierced length

The pierced length was found by multiplying the bubble velocity by the local bubble residence time. The relative frequency polygon for the pierced lengths calculated using the probe information is compared to that of the observed pierced lengths in Figure 5 for one $U/U_{mf}=1.4$ run. The agreement is excellent considering the uncertainty inherent in the observed values.

Characteristic bubble diameter

The pierced length distribution can be used to calculate a characteristic bubble diameter. Bubbles of varying sizes traverse the probe and the probe detects a pierced length equal to or less than the bubble diameter. For the case of a 2-D bed, the bubbles have an approximately circular cross-section and this shape will be assumed here. For 3-D beds, appropriate bubble shapes can be assumed such as those suggested by Tsutsui and Miyauchi (1980). The relationship between $\phi(y)$, the pierced length probability density function, and $f(d)$, the circle diameter probability density function is as follows (Reid, 1955):

$$f(d)=\frac{1}{\pi d}\int_{\infty}^{d} y(y^2-d^2)^{-1/2}\phi'(y)dy \tag{3}$$

Replacing the lower bound with d_{max}, the maximum pierced length measured, results in an equivalent integral. The value of d corresponding to the maximum value of $f(d)$ is the most probable (characteristic) circle diameter d_{char}. Because ϕ is calculated using the pierced length data, its values are discrete and the integration in Eq. 3 is done numerically. Since f depends on the derivative of the discrete function ϕ, ϕ was first smoothed using a low-pass filter. Also, because a large number of pierced lengths were required to accurately determine f, the pierced lengths from the five different runs at each fluidization velocity ratio were lumped together to calculate ϕ. Observed bubble diameters d_{eq} were calculated using the following relation:

$$d_{eq}=\sqrt{\frac{\pi}{4}A_{bub}} \tag{4}$$

where A_{bub} is the observed bubble area. The calculated characteristic bubble diameter is shown in comparison to the relative frequency polygon of observed values for $U/U_{mf}=1.4$ in Figure 6. Note that the characteristic bubble diameter overpredicts the average observed bubble diameter. This is due not only to the uncertainty inherent in the observations, but also because the assumed bubble shape is not always accurate. As noted by Geldart and Cranfield (1972), long, thin and horizontal bubbles exist close to the distributor plate growing into circles further up in the bed. For $U/U_{mf}=1.4$ in this 2-D bed, the lower probe is located in the transition region between the long, thin bubbles and the circular bubbles. When the probe is intercepting long, thin horizontal bubbles, the average d_{eq} will be greater than d_{char}.

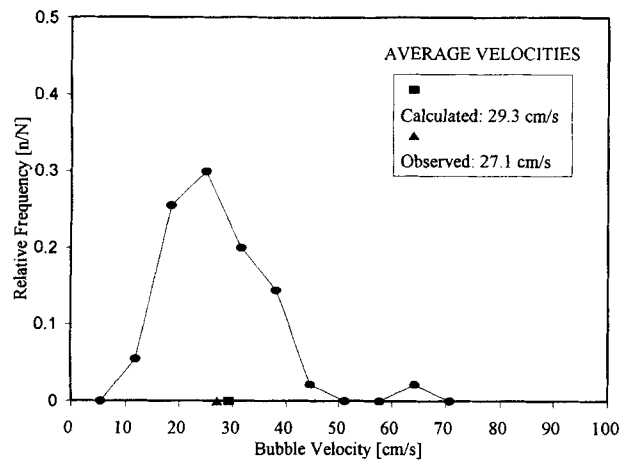

Figure 4. Observed bubble velocity relative frequency polygon.

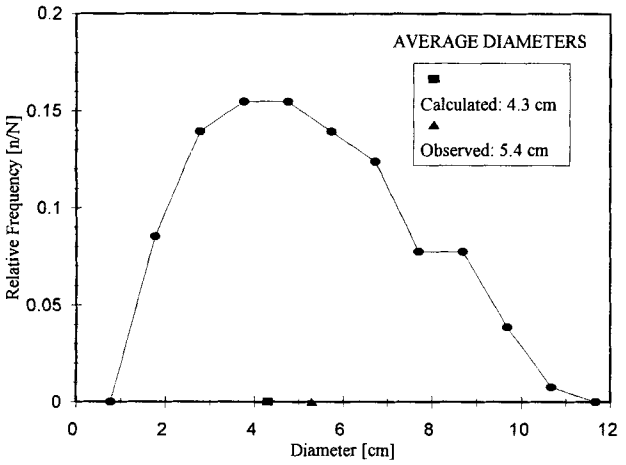

Figure 6. Observed bubble diameter relative frequency polygon.

Visible bubble flow

The visible bubble flow Q_b is the volume of gas that is carried by the rising bubbles across a horizontal plane per unit time in the bed assuming no gas flows through the bubble. For a circular bubble with characteristic calculated diameter d_{char} randomly pierced by the probe, the average pierced length is:

$$\bar{y} = \frac{\pi}{4} d_{char} \tag{5}$$

Assuming uniform bubble distribution across the width of the bed, the visible bubble flow across a horizontal plane including the probe is:

$$Q_b = f \bar{y} T W \tag{6}$$

where f is the bubble frequency measured at a point by the probe, T is the bed thickness and W is the bed width. Combining Eqs. 5 and 6 results in the following relation:

$$Q_b = \frac{\pi}{4} f d_{char} T W \tag{7}$$

Note that if the bubble shape had been assumed to have a semicircular cross-section, the value of d corresponding to the maximum in $f(d)$, d_{char}, would be the most probable semicircle radius. Although a semicircular cross-section with radius d_{char} has twice the area of a circular cross-section with diameter d_{char}, it is also twice as likely to be detected, resulting in equivalent $\bar{y}$ and visible bubble flow for either assumed shape.

Conclusions

An optical probe suitable for high temperature operation has been introduced and the methodology for processing the probe signal has been developed. The probe signal processing methodology consists of the use of a low-pass filter and an amplitude-cutoff filter. The probe can be used to determine bubble properties such as bubble frequency, local bubble residence time, bubble velocity, pierced length, characteristic bubble size, and visible bubble flow. The interpretation of the probe signal and the resulting bubble properties were confirmed by a visual check with videotape of the 2-D bed. With these procedures developed, the optical probe can be used in applications where visual observation is not possible.

Acknowledgments

The authors thank Sean Kopczynski and Lisa Freeman for their work on the 2-D bed facility leading to their MSME degrees and Dr. Alan George for his work developing the optical probe hardware. The financial support from the National Science Foundation (Grant Number CTS-8803077) for these contributions is gratefully acknowledged. The financial support in the form of graduate fellowships from the Dept. of Defense (National Defense Science and Engineering Graduate Fellowship Program), the Oregon Space Grant Fellowship Program, and the Dept. of Energy (Integrated Manufacturing Predoctoral Fellowship Program) is greatly appreciated.

Notation

$f(d)$ = bubble diameter probability density function
$H(s)$, $H(\omega)$ = transfer function for low-pass filter
y = pierced length variable for ϕ
$\bar{y}$ = average pierced length for a randomly pierced circular bubble

Greek letters

$\phi'(y)$ = derivative of $\phi(y)$ with respect to y
ω = frequency
ω_{cut} = cutoff frequency for first-stage (low-pass) filter

Literature Cited

Cranfield, R. R., "A Probe for Bubble Detection and Measurement in Large Particle Fluidised Beds," *Chem. Eng. Sci.*, **27**, 239 (1972).
De Lasa, H., S. L. P. Lee and M. A. Bergougnou, "Bubble Measurement in Three-Phase Fluidized Beds Using a U-Shaped Optical Fiber," *Can J. Chem. Eng.*, **62**, 165 (1984).
Dutta, S., and C. Y. Wen, "A Simple Probe for Fluidized Bed Measurement," *Can. J. Chem. Eng.*, **57**, 115 (1979).
Doebelin, E. O., *Measurement Systems: Application and Design*, 4th ed., p. 157 (1990).
Geldart, D., "The Size and Frequency of Bubbles in Two- and Three-dimensional Gas-Fluidised Beds," *Powder Technol.*, **4**, 41 (1970).
Geldart, D., and R. R. Cranfield, "The Gas Fluidisation of Large Particles," *Chem. Eng. J.*, **3**, 211 (1972).
Geldart, D., and J. R. Kelsey, "The Use of Capacitance Probes in Gas Fluidised Beds," *Powder Technol.*, **6**, 45 (1972).
Grace, J. R., and D. Harrison, "The Behavior of Freely Bubbling Fluidised Beds," *Chem. Eng. Sci.*, **24**, 497 (1969).
Gunn, D. J., and H. H. Al-Doori, "The Measurement of Bubble Flows in Fluidized Beds by Electrical Probe," *Int. J. Multiphase Flow*, **11**, 535 (1985).
Hager, W. R., and W. J. Thomson, "Bubble Behavior Around Immersed Tubes in a Fluidized Bed," *AIChE Symp. Ser.*, 69, 68 (1973).
Johnson, D. E., *Introduction to Filter Theory*, Prentice-Hall, Englewood Cliffs, NJ, p. 43 (1976).
Kunii, D., K. Yoshida, and I. Hiraki, "The Behavior of Freely Bubbling Fluidized Beds," *Proc. Int. Symp. on Fluidization*, A. A. H. Drinkenburg, ed., Netherlands Univ. Press, Amsterdam, p. 243 (1967).
Lockett, M. J., J. F. Davidson, and D. Harrison, "On the Two-Phase Theory of Fluidisation," *Chem. Eng. Sci.*, **22**, 1059 (1967).
Lord, W. K., G. McAndrews, M. Sakagami, J. A. Valenzuela, and L. R. Glicksman, "Measurement of Bubble Properties in Fluidized Beds," *Proc. Int. Fluidized Bed Comb. Conf.*, **1**, 76 (1982).

Masson, H., and R. Jottrand, "Measurement of Local Bubble Properties in a Fluidized Bed," *Fluidization*, J. F. Davidson and D. L. Keairns, eds., Cambridge Univ. Press, New York, p. 1 (1978).
Matsuura, A., and L. Fan, "Distribution of Bubble Properties in a Gas-Solid-Liquid Fluidized Bed," *AIChE J.*, **30**, 894 (1984).
Park, W. H., W. K. Kang, C. E. Capes, and G. L. Osberg, "The Properties of Bubbles in Fluidized Beds of Conducting Particles as Measured by an Electroresistivity Probe," *Chem. Eng. Sci.*, **24**, 851 (1969).
Partridge, B. A, and P. N. Rowe, "Analysis of Gas Flow in a Bubbling Fluidised Bed When Cloud Formation Occurs," *Trans. Inst. Chem. Eng.*, **44**, 349 (1966).
Press, W. H., B. P. Flannery, S. A. Teukolsky, and W. T. Vetterling, *Numerical Recipes: The Art of Scientific Computing (Fortran Version)*, Cambridge Univ. Press, New York, p. 415 (1989).
Reid, W. P., "Distribution of Sizes of Spheres in a Solid from a Study of Slices of the Solid," *J. of Math. and Phys.*, XXXIV, 95 (1955).
Rowe, P. N., and H. Masson, "Interaction of Bubbles with Probes in Gas Fluidised Beds," *Trans. Instn. Chem. Eng.*, **59**, 177 (1981).
Rowe, P. N., and B. A. Partridge, "An X-Ray Study of Bubbles in Fluidised Beds," *Trans. Instn. Chem. Engrs.*, **43**, 157 (1965).
Toomey, R. D., and H. P. Johnstone, "Gaseous Fluidisation of Solid Particles," *Chem. Eng. Sci.*, **48**, 220 (1952).
Tsutsui, T., and T. Miyauchi, "Fluidity of a Fluidized Catalyst Bed and Its Effect on the Behavior of the Bubbles," *Int. Chem. Eng.*, **20**, 386 (1980).
Walker, S. W., *Fast Fourier Transforms*, CRC Press, Boston, p. 14 (1991).
Weihong, L., B. Guangxiang, Z. Zengrong, Y. Jianhua, and C. Kefa, "Measurements of Bubble and Particle Motion in a Two-Dimensional FB," *Int. Conf. Fluidized Bed Comb.*, **2**, 1198 (1987).
Werther, J., "Bubbles in Gas Fluidised Beds: I," *Trans. Instn. Chem. Eng.*, **52**, 149 (1974).
Werther, J., and O. Molerus, "The Local Structure of Gas Fluidized Beds: I. A Statistically Base Measuring System," *Int. J. Multiphase Flow*, **1**, 103 (1973).
Yasui, G., and L. N. Johanson, "Characteristics of Gas Pockets in Fluidized Beds," *AIChE J.*, **4**, 445 (1958).
Yoshida, K., J. Sakane, and F. Shimizu, "A New Probe for Measuring Fluidization Bed Characteristics at High Temperatures," *Ind. Eng. Chem. Fundam.*, **21**, 85 (1982).